



Lung Segmentation from Chest X-Ray Images Using Deeplabv3plus-Based CNN Model

Dathar Abas Hasan ^{1,2}, Adnan Mohsin Abdulazeez ³

dathar.hasan@dpu.edu.krd, adnan.mohsin@dpu.edu.krd

¹ IT Department, Technical College of Informatics, Akre University of Applied Sciences, Duhok, Iraq.

² IT Dept., College of Health and Medical Technology-Shekhan, Duhok Polytechnic University, Duhok, Iraq.

³ Energy Eng. Dept., Technical College of Engineering, Duhok Polytechnic University, Duhok, Iraq.

Article Information

Submitted : 19 Jan 2024

Reviewed: 22 Jan 2024

Accepted : 8 Feb 2024

Keywords

Deep Learning, Lung segmentation, X-Ray, CNN, Semantic Segmentation

Abstract

As a result of technological advancements, a variety of medical diagnostic systems have grown rapidly to support the healthcare sectors. Over the past years, there has been considerable interest in utilizing deep learning algorithms for the proactive diagnosis of multiple diseases. In most cases, Coronavirus (COVID-19) and tuberculosis (TB) are diagnosed through the examination of pulmonary X-rays. Deep learning algorithms can identify tuberculosis with an almost medical-grade level of consistency by extracting the lung regions in the X-ray images. The probability of tuberculosis detection is increased when classification algorithms are applied to segmented lungs rather than the entire X-ray. The main focus of this paper is to execute lung segmentation from X-ray images using the deeplabv3plus CNN-based semantic segmentation model. In other CNN architectures, the feature resolution diminishes as the network becomes deeper due to the use of sequential convolutions with pooling or striding within the down-sampling stage. To tackle this drawback, deeplabv3plus incorporates "Atrous Convolution" in addition to modifying the pooling and convolutional striding components of the backbone. The experimental results were: an accuracy of 97.42%, a Jaccard index of 93.49%, and a dice coefficient of 96.63%. We also conduct an extensive comparison between the deeplabv3plus segmentation model and other benchmark segmentation architectures. The results prove the ability of the deeplabv3plus model to achieve precise lung segmentation from X-ray images.

A. Introduction

Chest X-rays are primarily used to diagnose different cardiac and pulmonary conditions by examining the anatomical structures of the chest, including the heart, clavicles, and lungs [1]. In the healthcare sector, many chest X-ray images are generated annually to examine the medical cases of patients [2][3]. This excessive increase requires effort, high costs, and time to be analyzed manually. Nowadays, Computer-Aided Diagnostic (CAD) systems are widely used to detect multiple types of chest disease [4]. Recent years have seen a significant development in CAD systems to support radiologists in diagnosing chest radiographs [5]. Various analytical tasks that need accurate segmentation of the anatomical structures in the chest radiography images are considered when designing the CAD system [6][7]. These duties include estimating the presence of disease and doing different size measurements on the chest radiographs, such as identifying lung disease or pulmonary nodules using lung field segmentation [8]. Diagnosing radiographic chest images, however, remains difficult when it comes to bodily structures like the heart, clavicles, and lungs that have overlapping and hazy borders [9][10]. Furthermore, the gender, age, and physical characteristics of the patient affect the size and shape of anatomical structures. A further factor that complicates the segmentation of anatomical features in chest radiography is the existence of medical equipment, such as guidewires and pacemakers [11].

Semantic segmentation is considered one of the computer vision tasks in which each pixel is classified to its semantic label. In contrast to image classification, which classifies the whole image into a single label [12]. The objective of semantic segmentation is to present a comprehensive understanding of the image at the pixel level. The main applications of semantic segmentation are auto-driving systems, medical image analysis, object detection, and scene understanding [13]. The traditional image segmentation techniques often depend on low-level features, such as edges or textures, to separate objects in an image [14][15]. Rule-based systems, such as intensity thresholding, edge detection-based techniques, hybrid models, and landmark-based models are some examples of these strategies [16]. Unfortunately, the effective performance of these approaches depends on optimizing some parameters, and they often are not precise when the anatomical parts overlap [17].

Deep learning and Convolutional Neural Networks (CNNs) have made significant advancements in semantic segmentation. CNNs perform exceptionally well in segmentation tasks, particularly in biomedical imaging, which is why CNN-based approaches have become widely used [18]. Additionally, medical applications such as vascular segmentation, catheter segmentation in X-rays, and lung segmentation in chest radiography have benefited greatly from deep learning [19]. The deep learning techniques that are most used in segmentation tasks are Fully Connected Network (FCN), U-Net, and Residual CNN (Res-Net) [20]. Nevertheless, it can be challenging to segment the medical images using U-Net22 since the Region of Interest (ROI) may look similar. To get a more accurate segmentation performance, deeper CNN structures with more layers are preferred for better feature representation [21]. To obtain a better feature representation for the anatomical structure segmentation, we, therefore, used a residual CNN architecture with identity connection [22].

This paper aims to perform semantic lung segmentation from X-ray images using residual-based deeplabv3Plus. Then the proposed method has been evaluated by comparing it with some related works. The deeplabv3plus proved its robustness to achieve precise lung segmentation and extract the ROI.

The rest of this paper is organized as: section two presents a survey about the most related research that focused on the utilization of deep learning in lung segmentation. Section three describes the research methodology, dataset description, preprocessing, training environment, and deeplabv3plus architecture. Section Four provides and discusses the obtained results, and section five identifies the main conclusion points for this paper.

B. Related Works

Extracting the lung shapes from the X-ray images is a crucial task in medical image diagnosis. A variety of diseases can be identified and treated depending on the lung shape. Hence, many researchers focused on studying and developing many deep learning-based techniques to achieve this task.

W. Liu et al. proposed an enhanced U-Net model to segment lung shapes from X-ray images. The model is trained and tested using the Japanese Society of Radiological Technology (JSRT) and Montgomery County (MC) datasets. The enhancement involves utilizing an efficientNet-b4 as an encoder and the residual block with ReLU activation function to work as a decoder. The evaluation result indicated the ability of the proposed system to optimize the traditional U-Net dice coefficient by 2.5% and the Jaccard index by 6% [23].

S. A. Hashem and M. Y. Kamil used a traditional U-Net model with contracting encoder and decoder paths to segment the lung regions from 565 images with its masks in Shenzhen and Montgomery publicly available datasets. ADAM was employed as an optimization algorithm because it involves the advantages of RMSProp and AdaGrad. The experimental results of the proposed model were in terms of accuracy 91.47 and IoU 74.94% [24].

S. Gite et al, investigated some segmentation benchmarks such as FCN, Seg-Net, U-Net, and U-Net++ to use in lung segmentation from X-rays. Detection and classification of tuberculosis can be more accurate after lung segmentation. Consequently, the U-Net ++ performance in lung segmentation was compared with the performance of the rest segmentation models. The U-Net ++ has achieved a higher accuracy of 98% and a mean IoU of 95% [25].

T. Pranata et al. proposed a traditional U-Net CNN model to segment the lung shape from X-ray images in the MC and Shenzhen datasets. The images have been preprocessed using Contrast Limited Adaptive Histogram Equalization (CLAHE) to be sufficient for model training. The effectiveness of the model is examined and the results are measured in terms of average accuracy of 91.68, sensitivity of 92.80%, precision of 95.07%, and F1 score of 93.92% [26].

P. R. A. S. Bassi and R. Attux investigated the importance of the lung segmentation process in generalizing the COVID-19 states classification. The traditional U-Net has been used to segment X-ray images from NIH ChestX-ray14, Montgomery and Shenzhen, the Covid-19 dataset, and CheXPert datasets. The classification has been performed with and without lung, segmentation to check the impact of segmentation on the classification results. The result showed that

classification mean accuracy was 78.7% with segmentation and 74% without segmentation [27].

M. Chavan et al. proposed a ResUNet++ segmentation model by composing traditional Res-Net and U-Net. The ResUNet++ involved contracting the encoder and expanding the decoder as well as using the identity connection of the Res-Net. The Montgomery dataset with 138 images was used and preprocessed to be valid for training. The proposed model was evaluated by comparing its performance with the performance of the FCN, U-Net, Res-Net, and Seg-Net. The ResUNet++ achieved a higher Dice coefficient of 96.26%, and a higher IoU of 94.27% [28].

Y. Said et al. developed a segmentation and classification diagnosing system to detect lung cancer cases in Decathlon 3D CT scans. The proposed system has two parts: the segmentation involves modifying U-Net to build the UNETR model and classification of the segmented CT scans to benign or malignant cases. The proposed system presented a segmentation accuracy of 97.83% and a classification accuracy of 98.77% [29].

Y. Lyu and X. Tian suggested the "Multiple tasking Wasserstein Generative Adversarial Network (MWG-UNet)" model to tackle the vanishing gradient issues in GAN networks. The model segmented the lung field and heart regions from JSRT dataset images. Data augmentation and adaptive histogram equalization were used as a preprocessing operation to increase and enhance the input images. The segmentation results for lung fields and heart were dice coefficient 71.16%, and IoU 74.56%. At the same time, the lung field segmentation achieved 85.18% dice coefficient and 81.36% IoU. The obtained results indicated that the model needs to be improved to segment accurately [30].

I. Ullah et al. developed a multi-organs segmentation framework to analyze the chest's anatomical structure in the X-ray images. This framework used two encoder-decoder-based networks. The first network used predefined VGG19, the output of the first network is fed as input of the second network which is designed based on the recurrent residual blocks to increase the performance of the small parts segmentation. The framework was evaluated using three datasets MC, JSRT, and SCXR separately in terms of the Dice coefficient and IoU [31].

D. Hasan and U. Jader utilized the predefined Seg-Net as a semantic segmentation model to segment the lung regions from X-ray images. The model was evaluated using 539 images from MC and Shenzhen publicly available datasets. The X-ray images have been preprocessed and resized to 256*256 to be suitable for model training and testing. The experimental results were (97.71%) as dice coefficient and (94.08%) as IoU [32].

A. Sulaiman et al. presented a concatenated block based on CNN to segment lung pixels from X-ray images. Each block contains a set of kernels that extract the important features from the images. To examine the robustness of the model, five datasets (MC, have been used to train and test the model. The performance of the model is measured in accuracy at 97%, IoU of 93%, and 96% of the Dice coefficient [33].

A. E. Pedersen et al. investigated the ability of the U-Net CNN to be utilized in lung segmentation and optimized collimation borders on a limited X-ray dataset. The 672 X-ray images from the Shenzhen dataset have been used and resized to three different dimensions 128*128, 256*256, and 512*512. The U-Net has been

trained and tested using each image dimension set separately. Then, the generated masks were compared with the handcrafted images by three radiographers and two junior radiologists. This comparison was performed using the Disc coefficient, which indicated that U-Net can present accurate lung segmentation from X-ray images [34].

C. Methodology

a. Dataset

In this paper, Shenzhen's publicly available dataset has been utilized to train, evaluate, and test the performance of a state-of-art deeplabv3plus segmentation model. The dataset is collected and validated in cooperation with Shenzhen No. 3 People's Hospital, Guangdong Medical College, Shenzhen, China, the Shenzhen dataset. It consists of 662 X-ray images for various cases that come from outpatient clinics and were taken with a Philips DR Digital Diagnose system as part of the regular hospital protocol within a month, primarily in September 2012. The dataset includes frontal chest X-rays, including pediatric X-rays (AP), 326 of which are normal cases and 336 of which show signs of tuberculosis. Although it can vary, their approximate dimension is $3K \times 3K$ pixels.

b. Data Preprocessing

Since the X-ray images in the Shenzhen dataset are in JPEG and DICOM formats, as well as, the dimensions of the images are not unified, the X-ray images were converted to PNG format to make the model's training faster and easier. Next, the dimensions of the input images have been resized to $256 * 256$ to be valid for the input layer. The data augmentation technique is an essential tool to enrich the dataset images. Many data augmentation techniques have been such as rotation, scaling, and reflection to provide the dataset with additional samples for training operations. The dataset has been divided into 60% for training, 30% for testing, and 10% for the. After preprocessing the X-ray images, the number of pixels in training dataset images was distributed on the two classes, Image background and the ROI (lung) as shown in Table 1.

Table 1. Pixel Distribution on the Background and Lung Regions.

Name	Pixel Count	Image Pixel Count
Background	2.7373×10^7	3.6635×10^7
Lung	9.2614×10^6	3.6635×10^7

Figure 1 shows the number of pixels for each class in the training dataset.

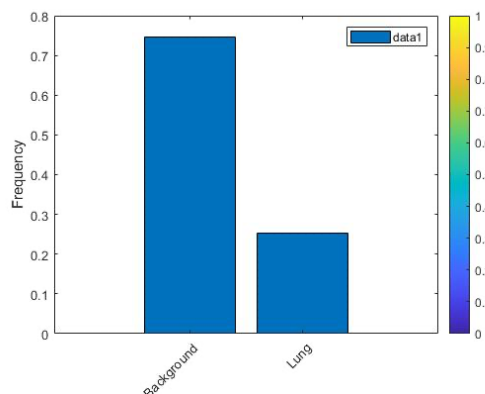


Figure 1. Pixel Distribution in Training Dataset.

c. DeepLabv3Plus Model

Google Artificial Intelligence designed a set of high-performing traditional deep-learning semantic segmentation networks called Deeplab. The most advanced model in this series, Deeplabv3plus, is an enhanced version of Deeplabv3. Many autonomous driving firms use this practical technology for lane detection and environment perception because of its ability to restore image features, which results in high output image performance. Despite the extensive and intricate network design, the semantic segmentation effect essentially has no flaws. The expanded convolution is used by the backbone network in the encoder of this network to expand the receptive field and enhance information feature extraction performance.

The decoder receives the low-level features from the backbone network, and an Atrous Spatial Pyramid Pooling (ASPP) module combines the high-level semantic features to improve the image's global semantic information. The ASPP performs the convolutional operation on the feature map using a convolution kernel with varying expansion rates, improving the capability of global feature learning. The Concat function in the network decoder fuses the ASPP output with low-level features, and a sequence of convolution layers and up-sampling brings the image back to the original resolution. Figure 2 shows the architecture of the encoder and decoder in deeplabv3plus.

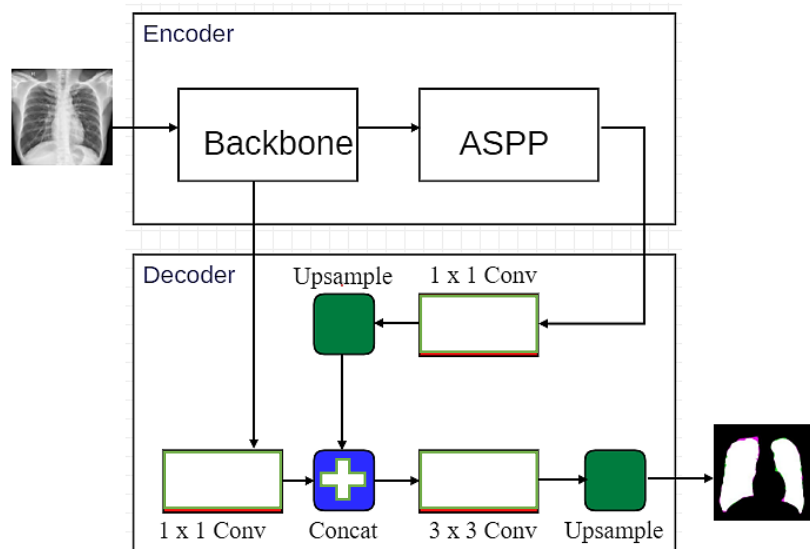


Figure 2. DeepLabv3Plus Architecture.

In the Backbone module, to optimize the segmentation labels from the input images, deeplabv3 has been enhanced by adding an effective decoder module. With faster calculation, DeepLabV3+ further improves performance by using a modified version of the "Aligned Xception" model as its main feature extractor. The modified backbone substitutes depth-wise separable convolutions for all down-sampling max pooling blocks; it does not update the "entry flow" like its counterpart. This makes extracting feature maps at any resolution possible by utilizing the suggested Atrous separable convolution. Beyond each (3×3) depth-wise separable convolution, there is a batch normalization and a ReLU activation layer.

d. Model Training

We have presented the configuration of the hyperparameters that have produced the best results after running tests with many values for hyperparameters. With deeplabv3plus, we have utilized a batch size of 1. The early layers of deep learning neural networks handle generic characteristics, suggesting that they may be applied to tasks other than random weight initialization in computer vision. We have applied the Adam optimization method with a learn rate drop period of 1, a learning rate drop factor of 0.3, and an initial learn rate of 0.001. Because of a binary class issue, the sigmoid cross entropy loss function was used to train all networks for 15 epochs. The training process has been executed using an ASUS computer system, i5 CPU with 8 cores, 8 GB of RAM Windows 11 operating system, and 2GB NVIDIA GeForce MX 110 GPU with 2. This study was carried out using the MATLAB. However, the model takes about (1) hour and (21) minutes to be trained and tested.

D. Result and Discussion

Many evaluation metrics have been used to evaluate the performance of the Seg-Net semantic segmentation model, including the Jaccard index, Dice Similarity Coefficient (DSC), and Global Accuracy. As illustrated in the subsequent expression, the global accuracy is typically calculated as the proportion of accurately predicted pixels within all labels in the testing dataset to the total number of pixels.

$$\text{Global Accuracy} = (\text{TN} + \text{TP}) / (\text{TP} + \text{TN} + \text{FN} + \text{FP}) \quad (1)$$

Where TP is the number of the predicted pixels that are truly predicted as a background, TN is the number of the pixels that are predicted as truly a lung. FP is the number of pixels in background regions but predicted as lung pixels, and FN is the number of pixels in lung regions but predicted as background pixels. The Dice Coefficient is usually used as an indicator of the overlapping area between the actual label and the predicted label as expressed in the following:

$$\text{Dice Coefficient} = (2 * \text{TP}) / ((\text{TP} + \text{FP}) + (\text{FN} + \text{TP})) \quad (2)$$

Another evaluation metric is the Intersection Over Union (IoU) metric which is known as the Jaccard index. It is considered as a similarity index between the ground truth and predicted labels. The following formula expresses the IoU:

$$\text{Intersection over Union (Jaccard Index)} = \text{TP} / (\text{TP} + \text{FN} + \text{FP}) \quad (3)$$

The confusion matrix shown in Table 2 illustrates that about 98.6% of the background pixels have been truly predicted as background, while about 1.3% of the background pixels have been predicted falsely as lung. In addition, there is about 93.8% of the lung pixels have been truly predicted as lung and about 6.1% have been predicted falsely as background.

Table 2. Confusion Matrix of The Deeplabv3plus Performance.

	Background	Lung
Background	0.98656	0.013438
Lung	0.061239	0.93876

To visualize the pixels that have been predicted as background and lung, we overlay the actual class label of the X-ray image with its corresponding predicted class label as shown in Figure 3.

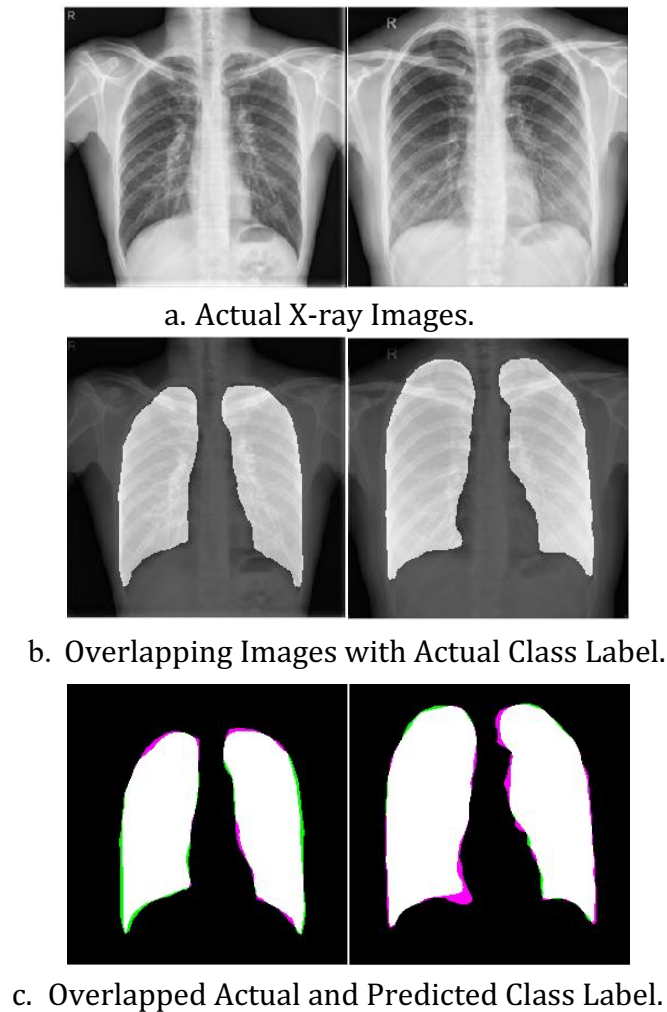


Figure 3. The Actual and Predicting Class.

The black and white regions in Figure 3-c refer to the background and lung regions respectively. The black and white regions appear as a result of successfully predicting the pixels for the background and lung. The green color refers to the pixels that belong to the lung class but are predicted as background pixels. Similarly, the violet color refers to the background pixels but is predicted as lung.

The experimental results of the proposed deeplabv3plus are illustrated in Table 2 as shown below:

Table 3. The Experimental Results of The Proposed Deeplabv3plus Model.

Metric	Value
Dice Coefficient (DC)	0.9663
Jaccard Index (JI)	0.9349
Global Accuracy (GA)	0.9742

The effectiveness of the proposed deeplabv3plus model to perform accurate segmentation is compared with other state-of-the-art models in terms of some

performance criteria. Table 4 compares the performance of the proposed model with other related works.

Table 4. Comparison of The Proposed Work with The Related Works.

Author	Model	Dataset	GA	JI	Dice
S. A. Hashem and M. Y. Kamil [24]	U-Net	Shenzhen	91.47%	74.94	-
T. Pranata et al. [26]	U-Net	MC and Shenzhen	91.68	-	-
M. Chavan et al. [28]	ResNet with U-Net	MC	-	94.27%	96.26%
Y. Lyu and X. Tian [30]	MWG-UNet	JSRT	-	81.36%	85.18%
A. Sulaiman et al. [33]	CNN	MC	97%	93%	96%
The Proposed Work (Deeplabv3plus)	Deeplabv3plus	Shenzhen	97.42%	93.49%	96.63%

In comparison with other related models, deeplabv3plus achieved better performance than other works. Many works utilized the U-Net with MC and Shenzhen datasets as the model can be trained and tested with small datasets

E. Conclusion

This research proposed an automated deeplabv3plus CNN model to accurately segment the region of interest in X-ray images. This model is capable of distinguishing the pixels' classes within fuzzy regions that separate the lung regions from the image background. Precise segmentation of lung segmentation is a significant step towards building a robust CAD system that supports medical decisions about the various types of chest diseases. The ASPP module gives the deeplabv3plus model the ability to improve the image's global semantic information by combining the high-level semantic features. In addition, the performance of the deeplabv3plus has been optimized using a modified version of the "Aligned Xception" model as its main feature extractor. The performance of the model has been measured and compared with other related works. The results indicate the ability of the proposed system to execute accurate semantic lung segmentation from X-ray images. We recommend that the deeplabv3plus model be modified using transfer learning to increase the performance as well as minimize the number of parameters to reduce the time required to train the model.

F. References

- [1] W. Al-Zyoud, D. Erekat, and R. Saraiji, "COVID-19 chest X-ray image analysis by threshold-based segmentation," *Heliyon*, vol. 9, no. 3, p. e14453, 2023, doi: 10.1016/j.heliyon.2023.e14453.
- [2] T. Agrawal and P. Choudhary, "Segmentation and classification on chest radiography: a systematic survey," *Vis. Comput.*, vol. 39, no. 3, pp. 875–913, 2023, doi: 10.1007/s00371-021-02352-7.
- [3] A. Das, *Adaptive UNet-based Lung Segmentation and Ensemble Learning with CNN-based Deep Features for Automated COVID-19 Diagnosis*, vol. 81, no. 4. Springer US, 2022. doi: 10.1007/s11042-021-11787-y.

-
- [4] L. Alzubaidi *et al.*, *Review of deep learning: concepts, CNN architectures, challenges, applications, future directions*, vol. 8, no. 1. Springer International Publishing, 2021. doi: 10.1186/s40537-021-00444-8.
- [5] A. F. Jahwar and A. M. Abdulazeez, "Segmentation and Classification for Breast Cancer Ultrasound Images Using Deep Learning Techniques: A Review," in *2022 IEEE 18th International Colloquium on Signal Processing & Applications (CSPA)*, 2022, pp. 225–230. doi: 10.1109/CSPA55076.2022.9781824.
- [6] P. B. Chanda and S. K. Sarkar, "Effective and Reliable Lung Segmentation of Chest Images with Medical Image Processing and Machine Learning Approaches," *Proc. IEEE Int. Conf. Advent Trends Multidiscip. Res. Innov. ICATMRI 2020*, 2020, doi: 10.1109/ICATMRI51801.2020.9398450.
- [7] G. M. M. Alshmrani, Q. Ni, R. Jiang, H. Pervaiz, and N. M. Elshennawy, "A deep learning architecture for multi-class lung diseases classification using chest X-ray (CXR) images," *Alexandria Eng. J.*, vol. 64, pp. 923–935, 2023, doi: 10.1016/j.aej.2022.10.053.
- [8] H. Dathar and A. M. Abdulazeez, "A Modified Convolutional Neural Networks Model for Medical Image Segmentation," *TEST Eng. Manag.*, vol. 83, no. July, pp. 16798–16808, 2020.
- [9] A. Haghanifar, M. M. Majdabadi, Y. Choi, S. Deivalakshmi, and S. Ko, *COVID-CXNet: Detecting COVID-19 in frontal chest X-ray images using deep learning*, vol. 81, no. 21. Multimedia Tools and Applications, 2022. doi: 10.1007/s11042-022-12156-z.
- [10] D. A. Zebari, D. Q. Zeebaree, A. M. Abdulazeez, H. Haron, and H. N. A. Hamed, "Improved Threshold Based and Trainable Fully Automated Segmentation for Breast Cancer Boundary and Pectoral Muscle in Mammogram Images," *IEEE Access*, vol. 8, pp. 203097–203116, 2020, doi: 10.1109/ACCESS.2020.3036072.
- [11] K. He, X. Zhang, S. Ren, and J. Sun, "Deep residual learning for image recognition," *Proc. IEEE Comput. Soc. Conf. Comput. Vis. Pattern Recognit.*, vol. 2016-Decem, pp. 770–778, 2016, doi: 10.1109/CVPR.2016.90.
- [12] M. M. Lotfy *et al.*, "Semantic Pneumonia Segmentation and Classification for Covid-19 Using Deep Learning Network," *Comput. Mater. Contin.*, vol. 73, no. 1, pp. 1141–1158, 2022, doi: 10.32604/cmc.2022.024193.
- [13] O. S. Kareem, A. K. AL-Sulaifanie, D. A. Hasan, and D. M. Ahmed, "Segmenting and Classifying the Brain Tumor from MRI Medical Images Based on Machine Learning Algorithms: A Review," *Asian J. Res. Comput. Sci.*, no. July, pp. 50–61, 2021, doi: 10.9734/ajrcos/2021/v10i230239.
- [14] M. Murugappan, A. K. Bourisly, N. B. Prakash, M. G. Sumithra, and U. R. Acharya, "Automated semantic lung segmentation in chest CT images using deep neural network," *Neural Comput. Appl.*, vol. 35, no. 21, pp. 15343–15364, 2023, doi: 10.1007/s00521-023-08407-1.
- [15] M. Muhammad, D. Zeebaree, A. M. A. Brifcani, J. Saeed, and D. A. Zebari, "A Review on Region of Interest Segmentation Based on Clustering Techniques for Breast Cancer Ultrasound Images," *J. Appl. Sci. Technol. Trends*, vol. 1, no. 3, pp. 78–91, 2020, doi: 10.38094/jastt1328.
- [16] R. Wang, T. Lei, R. Cui, B. Zhang, H. Meng, and A. K. Nandi, "Medical image

- segmentation using deep learning: A survey," *IET Image Process.*, vol. 16, no. 5, pp. 1243–1267, 2022, doi: 10.1049/ipr2.12419.
- [17] R. T. Wahyuningrum *et al.*, "Chest X-ray dataset and ground truth for lung segmentation," *Data Br.*, vol. 51, p. 109640, 2023, doi: 10.1016/j.dib.2023.109640.
- [18] J. Sousa *et al.*, "Lung Segmentation in CT Images: A Residual U-Net Approach on a Cross-Cohort Dataset," *Appl. Sci.*, vol. 12, no. 4, 2022, doi: 10.3390/app12041959.
- [19] K. Sharifani and M. Amini, "Machine Learning and Deep Learning: A Review of Methods and Applications," *World Inf. Technol. Eng. J.*, vol. 10, no. 07, pp. 3897–3904, 2023, [Online]. Available: <https://ssrn.com/abstract=4458723>
- [20] P. Malhotra, S. Gupta, D. Koundal, A. Zaguia, M. Kaur, and H. N. Lee, "Deep Learning-Based Computer-Aided Pneumothorax Detection Using Chest X-ray Images," *Sensors*, vol. 22, no. 6, 2022, doi: 10.3390/s22062278.
- [21] A. Mohammed and R. Kora, "A comprehensive review on ensemble deep learning: Opportunities and challenges," *J. King Saud Univ. - Comput. Inf. Sci.*, vol. 35, no. 2, pp. 757–774, 2023, doi: 10.1016/j.jksuci.2023.01.014.
- [22] T. Pang, S. Guo, X. Zhang, and L. Zhao, "Automatic lung segmentation based on texture and deep features of HRCT images with interstitial lung disease," *Biomed Res. Int.*, vol. 2019, 2019, doi: 10.1155/2019/2045432.
- [23] W. Liu, J. Luo, Y. Yang, W. Wang, J. Deng, and L. Yu, "Automatic lung segmentation in chest X-ray images using improved U-Net," *Sci. Rep.*, vol. 12, no. 1, pp. 1–10, 2022, doi: 10.1038/s41598-022-12743-y.
- [24] S. A. Hashem and M. Y. Kamil, "Segmentation of Chest X-Ray Images Using U-Net Model," *Mendel*, vol. 28, no. 2, pp. 49–53, 2022, doi: 10.13164/mendel.2022.2.049.
- [25] S. Gite, A. Mishra, and K. Kotecha, "Enhanced lung image segmentation using deep learning," *Neural Comput. Appl.*, vol. 35, no. 31, pp. 22839–22853, 2022, doi: 10.1007/s00521-021-06719-8.
- [26] T. Pranata, A. Desiani, B. Suprihatin, H. Hanum, and F. Efriliyanti, "Segmentation of the Lungs on X-Ray Thorax Images with the U-Net CNN Architecture," *Comput. Eng. Appl. J.*, vol. 11, no. 2, pp. 101–111, 2022, doi: 10.18495/comengapp.v11i2.404.
- [27] P. R. A. S. Bassi and R. Attux, "Covid-19 detection using chest X-rays: is lung segmentation important for generalization?," *Res. Biomed. Eng.*, vol. 38, no. 4, pp. 1121–1139, 2022, doi: 10.1007/s42600-022-00242-y.
- [28] M. Chavan, V. Varadarajan, S. Gite, and K. Kotecha, "Deep Neural Network for Lung Image Segmentation on Chest X-ray," *Technologies*, vol. 10, no. 5, 2022, doi: 10.3390/technologies10050105.
- [29] Y. Said, A. A. Alsheikhy, T. Shawly, and H. Lahza, "Medical Images Segmentation for Lung Cancer Diagnosis Based on Deep Learning Architectures," *Diagnostics*, vol. 13, no. 3, 2023, doi: 10.3390/diagnostics13030546.
- [30] Y. Lyu and X. Tian, "MWG-UNet: Hybrid Deep Learning Framework for Lung Fields and Heart Segmentation in Chest X-ray Images," *Bioengineering*, vol. 10, no. 9, 2023, doi: 10.3390/bioengineering10091091.
- [31] I. Ullah, F. Ali, B. Shah, S. El-Sappagh, T. Abuhmed, and S. H. Park, "A deep

- learning based dual encoder–decoder framework for anatomical structure segmentation in chest X-ray images,” *Sci. Rep.*, vol. 13, no. 1, pp. 1–14, 2023, doi: 10.1038/s41598-023-27815-w.
- [32] D. Hasan and U. Jader, “Semantic Lung Segmentation from Chest X-Ray Images Using Seg-Net Deep CNN Model,” *Polytech. J.*, vol. 13, no. 2, 2023, doi: 10.59341/2707-7799.1712.
- [33] A. Sulaiman *et al.*, “A Convolutional Neural Network Architecture for Segmentation of Lung Diseases Using Chest X-ray Images,” *Diagnostics*, vol. 13, no. 9, 2023, doi: 10.3390/diagnostics13091651.
- [34] A. E. Pedersen, M. W. Kusk, G. H. Knudsen, C. A. G. R. Busk, and S. Lysdahlgaard, “Collimation border with U-Net segmentation on chest radiographs compared to radiologists,” *Radiography*, vol. 29, no. 3, pp. 647–652, 2023, doi: 10.1016/j.radi.2023.04.016.